JHEP

Published for SISSA by Springer

Received: April 16, 2013
Accepted: June 10, 2013
Published: July 8, 2013

Holographic fermionic liquid with lattices

Yi Ling,[a,b] **Chao Niu,**[a] **Jian-Pin Wu,**[c,d,e] **Zhuo-Yu Xian**[f,a] **and Hongbao Zhang**[g,h]

[a] *Institute of High Energy Physics, Chinese Academy of Sciences, Beijing 100049, China*

[b] *State Key Laboratory of Theoretical Physics, Institute of Theoretical Physics, Chinese Academy of Sciences, Beijing 100190, China*

[c] *Department of Physics, Hanyang University, Seoul 133-791, Korea*

[d] *Center for Quantum Spacetime, Sogang University, Seoul 121-742, Korea*

[e] *Department of Physics, School of Mathematics and Physics, Bohai University, Jinzhou 121013, China*

[f] *Department of Physics, South China University of Technology, Guangzhou 510641, China*

[g] *Theoretische Natuurkunde, Vrije Universiteit Brussel, Pleinlaan 2, B-1050 Brussels, Belgium*

[h] *The International Solvay Institutes, Pleinlaan 2, B-1050 Brussels, Belgium*

E-mail: lingy@ihep.ac.cn, niuc@ihep.ac.cn, jianpinwu@yahoo.com.cn, x.zhuoyu@mail.scut.edu.cn, hzhang@vub.ac.be

Abstract: We investigate the holographic fermions over a gravitational lattice background with a rather low temperature. Since the rotation symmetry is broken on the plane, the lattice effects change the shape of the Fermi surface within the first Brillouin zone from a circle to an ellipse. When the Fermi surface intersects with the Brillouin zone boundary, the band structure with a band gap is observed through a numerical analysis. We construct a lattice model sourced by a scalar field as well as an ionic lattice model without the scalar field. In both cases we find the similar physical results.

Keywords: Holography and condensed matter physics (AdS/CMT), Gauge-gravity correspondence

doi:10.1007/JHEP07(2013)045

JHEP07(2013)045

Contents

1 Introduction

As a powerful tool of understanding a variety of strongly coupled condensed matter systems, AdS/CMT has been entering an era from building purely theoretical models with highly symmetric configuration to modelling more realistic condensed matter system with less symmetry. In particular, instead of working within the probe limit, very recently the authors in [1] and [2] have constructed some spatially inhomogeneous but periodic gravitational backgrounds by fully solving the coupled partial differential equations numerically with the Einstein-DeTurck method. Such gravitational backgrounds, by holography, correspond to the boundary systems in the presence of a lattice, a key ingredient in the condensed matter systems. Thus with such gravitational backgrounds, one can explore various lattice effects in the holographic investigation of condensed matter systems. Actually for the transport coefficients such as optical conductivity and thermoelectric conductivity, it has been shown that not only does the presence of a lattice result in the Drude peak at low frequencies but also induces a new intermediate scaling regime in which a robust power law behavior is found with respect to the frequency [1, 2]. Remarkably such a result is in striking agreement with the experiments on the cuprates, including the superconducting phase [3].

The purpose of this paper is to investigate how such a holographic lattice affects the Fermi surface by putting the Dirac field in such bulk gravitational backgrounds. To achieve this, in the next section we first build up the holographic framework to extract the spectral function for fermions living on the boundary by solving the bulk Dirac equation in periodic backgrounds. Then we shall present a numerical construction of two kinds of ultra cold holographic lattices using the Einstein-DeTurck method in section III. After that, the numerical results for the Fermi surface in the presence of such holographic lattices are detailed in section IV. We shall conclude with some discussions as well as further directions in the final section.

JHEP07(2013)045

2 Holographic setup for the bulk Dirac field in periodic backgrounds

Start from the bulk action for a Dirac field with mass m and charge q

$$S_D = i\int d^4x\sqrt{-g}\bar{\zeta}\left(\Gamma^a\mathcal{D}_a - m\right)\zeta, \tag{2.1}$$

in the static background as general as

$$\begin{aligned} ds^2 &= -g_{tt}(x,z)dt^2 + g_{zz}(x,z)dz^2 + g_{xx}(x,z)dx^2 + g_{yy}(x,z)dy^2 + 2g_{xz}(x,z)dxdz, \\ A &= A_t(x,z)dt. \end{aligned} \tag{2.2}$$

Here $\Gamma^a = (e_\mu)^a\Gamma^\mu$ with $(e_\mu)^a$ a set of orthogonal normal vector bases and Γ^μ Gamma matrices. In addition, $\mathcal{D}_a$ is the covariant derivative, i.e.,

$$\mathcal{D}_a = \partial_a + \frac{1}{4}(\omega_{\mu\nu})_a\Gamma^{\mu\nu} - iqA_a, \tag{2.3}$$

where $\Gamma^{\mu\nu} = \frac{1}{2}[\Gamma^\mu, \Gamma^\nu]$, and $(\omega_{\mu\nu})_a$ are the spin connection 1-forms given by

$$(\omega_{\mu\nu})_a = (e_\mu)_b\nabla_a(e_\nu)^b. \tag{2.4}$$

With the following orthogonal normal vector bases

$$\begin{aligned} (e_0)^a &= \frac{1}{\sqrt{g_{tt}}}\left(\frac{\partial}{\partial t}\right)^a, \qquad (e_1)^a = \frac{1}{\sqrt{g_{xx}}}\left(\frac{\partial}{\partial x}\right)^a, \qquad (e_2)^a = \frac{1}{\sqrt{g_{yy}}}\left(\frac{\partial}{\partial y}\right)^a, \\ (e_3)^a &= -\sqrt{\frac{g_{xx}}{g_{xx}g_{zz} - g_{xz}^2}}\left(\frac{\partial}{\partial z}\right)^a + \frac{g_{xz}}{\sqrt{g_{xx}(g_{xx}g_{zz} - g_{xz}^2)}}\left(\frac{\partial}{\partial x}\right)^a, \end{aligned} \tag{2.5}$$

the non-vanishing components of spin connections can be calculated as follows

$$\begin{aligned} (\omega_{01})_a = -(\omega_{10})_a &= -\frac{\partial_x g_{tt}}{2\sqrt{g_{tt}g_{xx}}}(dt)_a, \\ (\omega_{03})_a = -(\omega_{30})_a &= \frac{g_{xx}\partial_z g_{tt} - g_{xz}\partial_x g_{tt}}{2\sqrt{g_{tt}g_{xx}(g_{xx}g_{zz} - g_{xz}^2)}}(dt)_a, \\ (\omega_{12})_a = -(\omega_{21})_a &= -\frac{\partial_x g_{yy}}{2\sqrt{g_{xx}g_{yy}}}(dy)_a, \\ (\omega_{13})_a = -(\omega_{31})_a &= \left(-\frac{\partial_z g_{xx}}{2\sqrt{g_{xx}g_{zz} - g_{xz}^2}} + \frac{2g_{xx}\partial_x g_{xz} - g_{xz}\partial_x g_{xx}}{2g_{xx}\sqrt{g_{xx}g_{zz} - g_{xz}^2}}\right)(dx)_a \\ &\quad + \frac{g_{xx}\partial_x g_{zz} - g_{xz}\partial_z g_{xx}}{2g_{xx}\sqrt{g_{xx}g_{zz} - g_{xz}^2}}(dz)_a, \\ (\omega_{23})_a = -(\omega_{32})_a &= \frac{g_{xz}\partial_x g_{yy} - g_{xx}\partial_z g_{yy}}{2\sqrt{g_{xx}g_{yy}(g_{xx}g_{zz} - g_{xz}^2)}}(dy)_a. \end{aligned} \tag{2.6}$$

Thus the Dirac equation

$$\Gamma^a\mathcal{D}_a\zeta - m\zeta = 0 \tag{2.7}$$

JHEP07(2013)045

can be written as

$$-\sqrt{\frac{g_{xx}}{g_{xx}g_{zz}-g_{xz}^2}}\Gamma^3\partial_z\zeta+\frac{1}{\sqrt{g_{tt}}}\Gamma^0(\partial_t-iqA_t)\zeta+\left(\frac{1}{\sqrt{g_{xx}}}\Gamma^1+\frac{g_{xz}}{\sqrt{g_{xx}(g_{xx}g_{zz}-g_{xz}^2)}}\Gamma^3\right)\partial_x\zeta$$
$$+\frac{1}{\sqrt{g_{yy}}}\Gamma^2\partial_y\zeta+\left(\frac{\partial_x g_{tt}}{4g_{tt}\sqrt{g_{xx}}}+\frac{\partial_x g_{yy}}{4g_{yy}\sqrt{g_{xx}}}+\frac{\sqrt{g_{xx}}\partial_x g_{zz}}{4(g_{xx}g_{zz}-g_{xz}^2)}+\frac{g_{xz}(g_{xz}\partial_x g_{xx}-2g_{xx}\partial_x g_{xz})}{4g_{xx}^{3/2}(g_{xx}g_{zz}-g_{xz}^2)}\right)$$
$$\times\Gamma^1\zeta-\frac{1}{4\sqrt{g_{xx}(g_{xx}g_{zz}-g_{xz}^2)}}\times$$
$$\times\left(\partial_z g_{xx}-2\partial_x g_{xz}+\frac{g_{xz}}{g_{xx}}\partial_x g_{xx}+\frac{g_{xx}\partial_z g_{tt}-g_{xz}\partial_x g_{tt}}{g_{tt}}+\frac{g_{xx}\partial_z g_{yy}-g_{xz}\partial_x g_{yy}}{g_{yy}}\right)\Gamma^3\zeta-m\zeta=0. \quad (2.8)$$

To proceed, let us first make a transformation $\zeta = (g_{tt}g_{xx}g_{yy})^{-\frac{1}{4}}\mathcal{F}$. Then the above equation turns out to be

$$-\sqrt{\frac{g_{xx}}{g_{xx}g_{zz}-g_{xz}^2}}\Gamma^3\partial_z\mathcal{F}+\frac{1}{\sqrt{g_{tt}}}\Gamma^0(\partial_t-iqA_t)\mathcal{F}+\left(\frac{1}{\sqrt{g_{xx}}}\Gamma^1+\frac{g_{xz}}{\sqrt{g_{xx}(g_{xx}g_{zz}-g_{xz}^2)}}\Gamma^3\right)\partial_x\mathcal{F}$$
$$+\frac{1}{\sqrt{g_{yy}}}\Gamma^2\partial_y\mathcal{F}+\left(-\frac{\partial_x g_{xx}}{4g_{xx}^{3/2}}+\frac{\sqrt{g_{xx}}\partial_x g_{zz}}{4(g_{xx}g_{zz}-g_{xz}^2)}+\frac{g_{xz}(g_{xz}\partial_x g_{xx}-2g_{xx}\partial_x g_{xz})}{4g_{xx}^{3/2}(g_{xx}g_{zz}-g_{xz}^2)}\right)\Gamma^1\mathcal{F}$$
$$+\frac{1}{4\sqrt{g_{xx}(g_{xx}g_{zz}-g_{xz}^2)}}\left(2\partial_x g_{xz}-2\frac{g_{xz}}{g_{xx}}\partial_x g_{xx}\right)\Gamma^3\mathcal{F}-m\mathcal{F}=0 \quad (2.9)$$

Next expanding $\mathcal{F}$ as $\mathcal{F}=F(x,z)e^{-i\omega t+ik_i x^i}$, one can have

$$\Delta_3\Gamma^3F+\Delta_0\Gamma^0F-\Delta_1\Gamma^1F-\Delta_2\Gamma^2F+mF=0, \quad (2.10)$$

where we have denoted

$$\Delta_3 =: \frac{1}{\sqrt{g_{xx}(g_{xx}g_{zz}-g_{xz}^2)}}\left(g_{xx}\partial_z-g_{xz}\partial_x-ik_1g_{xz}-\frac{1}{2}\partial_x g_{xz}+\frac{g_{xz}}{2g_{xx}}\partial_x g_{xx}\right),$$
$$\Delta_0 =: i(\omega+qA_t)\frac{1}{\sqrt{g_{tt}}},$$
$$\Delta_1 =: \left(\frac{1}{\sqrt{g_{xx}}}\partial_x+\frac{ik_1}{\sqrt{g_{xx}}}-\frac{\partial_x g_{xx}}{4g_{xx}^{3/2}}+\frac{\sqrt{g_{xx}}\partial_x g_{zz}}{4(g_{xx}g_{zz}-g_{xz}^2)}+\frac{g_{xz}(g_{xz}\partial_x g_{xx}-2g_{xx}\partial_x g_{xz})}{4g_{xx}^{3/2}(g_{xx}g_{zz}-g_{xz}^2)}\right),$$
$$\Delta_2 =: \frac{ik_2}{\sqrt{g_{yy}}}. \quad (2.11)$$

Now if we choose our gamma matrices as

$$\Gamma^3=\begin{pmatrix}-\sigma^3 & 0\\ 0 & -\sigma^3\end{pmatrix}, \qquad \Gamma^0=\begin{pmatrix}i\sigma^1 & 0\\ 0 & i\sigma^1\end{pmatrix},$$
$$\Gamma^1=\begin{pmatrix}-\sigma^2 & 0\\ 0 & \sigma^2\end{pmatrix}, \qquad \Gamma^2=\begin{pmatrix}0 & \sigma^2\\ \sigma^2 & 0\end{pmatrix}, \quad (2.12)$$

JHEP07(2013)045

and split the 4-component spinor into two 2-component spinors as $F = (F_1, F_2)^T$, then the Dirac equation becomes

$$\Delta_3 \begin{pmatrix} F_1 \\ F_2 \end{pmatrix} - m\sigma^3 \otimes \begin{pmatrix} F_1 \\ F_2 \end{pmatrix} + \Delta_0 \sigma^2 \otimes \begin{pmatrix} F_1 \\ F_2 \end{pmatrix} \pm i\Delta_1 \sigma^1 \otimes \begin{pmatrix} F_1 \\ F_2 \end{pmatrix} - i\Delta_2 \sigma^1 \otimes \begin{pmatrix} F_2 \\ F_1 \end{pmatrix} = 0. \quad (2.13)$$

Note that this is a coupled equation between F_1 and F_2 as opposed to the case in [4], where F_1 and F_2 are decoupled. Furthermore, by the decomposition

$$F_\alpha \equiv \begin{pmatrix} \mathcal{A}_\alpha \\ \mathcal{B}_\alpha \end{pmatrix} \quad (2.14)$$

with $\alpha = 1, 2$, the Dirac equation (2.13) can be expressed as

$$(\Delta_{30}\partial_z + \Delta_{31} \mp m) \begin{pmatrix} \mathcal{A}_1 \\ \mathcal{B}_1 \end{pmatrix} \mp i\Delta_0 \begin{pmatrix} \mathcal{B}_1 \\ \mathcal{A}_1 \end{pmatrix} + i\Delta_1 \begin{pmatrix} \mathcal{B}_1 \\ \mathcal{A}_1 \end{pmatrix} - i\Delta_2 \begin{pmatrix} \mathcal{B}_2 \\ \mathcal{A}_2 \end{pmatrix} = 0, \quad (2.15)$$

$$(\Delta_{30}\partial_z + \Delta_{31} \mp m) \begin{pmatrix} \mathcal{A}_2 \\ \mathcal{B}_2 \end{pmatrix} \mp i\Delta_0 \begin{pmatrix} \mathcal{B}_2 \\ \mathcal{A}_2 \end{pmatrix} - i\Delta_1 \begin{pmatrix} \mathcal{B}_2 \\ \mathcal{A}_2 \end{pmatrix} - i\Delta_2 \begin{pmatrix} \mathcal{B}_1 \\ \mathcal{A}_1 \end{pmatrix} = 0, \quad (2.16)$$

where

$$\begin{aligned} \Delta_{30} &=: \frac{g_{xx}}{\sqrt{g_{xx}(g_{xx}g_{zz} - g_{xz}^2)}}, \\ \Delta_{31} &=: \frac{-ik_1 g_{xz} - \frac{1}{2}\partial_x g_{xz} + \frac{g_{xz}}{2g_{xx}}\partial_x g_{xx}}{\sqrt{g_{xx}(g_{xx}g_{zz} - g_{xz}^2)}}. \end{aligned} \quad (2.17)$$

Suppose our background field is periodic along the x direction with the periodicity c. Then by the Bloch theorem, the solution to our Dirac equation can always be expanded as follows

$$\begin{pmatrix} \mathcal{A}_\alpha(x,z) \\ \mathcal{B}_\alpha(x,z) \end{pmatrix} = \sum_{n=0,\pm1,\pm2,\cdots} \begin{pmatrix} \mathcal{A}_{\alpha,n}(z) \\ \mathcal{B}_{\alpha,n}(z) \end{pmatrix} e^{inKx} \quad (2.18)$$

with $K = \frac{2\pi}{c}$.

Below we will restrict ourselves to the following periodic background, i.e.,

$$\begin{aligned} ds^2 &= \frac{1}{z^2}\{-(1-z)P(z)Q_{tt}(x,z)dt^2 + \frac{Q_{zz}(x,z)dz^2}{P(z)(1-z)} \\ &\quad + Q_{xx}(x,z)[dx + z^2 Q_{xz}(x,z)dz]^2 + Q_{yy}(x,z)dy^2\}, \\ A &= (1-z)\psi(x,z)dt. \end{aligned} \quad (2.19)$$

Here

$$P(z) = 1 + z + z^2 - \frac{\mu_1^2 z^3}{2} \quad (2.20)$$

with the other variables regular from the horizon $z = 1$ all the way to the conformal boundary $z = 0$. In particular, we require at the horizon

$$Q_{tt}(x,1) = Q_{zz}(x,1) \quad (2.21)$$

JHEP07(2013)045

and at the conformal boundary

$$Q_{tt}(x,0)=Q_{zz}(x,0)=Q_{xx}(x,0)=Q_{yy}(x,0)=1, Q_{xz}(x,0)=0, \psi(x,0)=\mu(x). \quad (2.22)$$

Hence such a geometry asymptotes AdS with the curvature radius $L=1$ and the temperature given by

$$T=\frac{P(1)}{4\pi}=\frac{6-\mu_1^2}{8\pi}. \quad (2.23)$$

With the above background ansatz, our Dirac equation gives rise to

$$\partial_z \begin{pmatrix} \mathcal{A}_{\alpha,n} \\ \mathcal{B}_{\alpha,n} \end{pmatrix} \pm \frac{\omega}{4\pi T}\frac{1}{1-z}\begin{pmatrix} \mathcal{B}_{\alpha,n} \\ \mathcal{A}_{\alpha,n} \end{pmatrix}=0 \quad (2.24)$$

at the horizon. In order to obtain the retarded Green function on the boundary by holography, the independent ingoing boundary condition should be imposed at the horizon, i.e.,

$$\begin{pmatrix} \mathcal{A}_{\alpha,n} \\ \mathcal{B}_{\alpha,n} \end{pmatrix}=\begin{pmatrix} 1 \\ -i \end{pmatrix}(1-z)^{-\frac{i\omega}{4\pi T}} \quad (2.25)$$

for each α and n with the others turned off. On the other hand, near the AdS boundary, our Dirac equation reduces to

$$(z\partial_z - m\sigma^3)\otimes\begin{pmatrix} F_{1,n} \\ F_{2,n} \end{pmatrix}=0\ . \quad (2.26)$$

Hence the solution can be asymptotically expanded near the AdS boundary as

$$F_{\alpha,n}\approx a_{\alpha,n}z^m\begin{pmatrix} 1 \\ 0 \end{pmatrix}+b_{\alpha,n}z^{-m}\begin{pmatrix} 0 \\ 1 \end{pmatrix}. \quad (2.27)$$

Holography tells us that the retarded Green function can be obtained by the following relation

$$a_{\alpha,n}(\beta,l)=G_{\alpha,n;\alpha',n'}b_{\alpha',n'}(\beta,l), \quad (2.28)$$

where $a_{\alpha,n}(\beta,l)$ and $b_{\alpha,n}(\beta,l)$ are the asymptotic expansion coefficients in (2.27) of the solution to the Dirac equation evolving from the ingoing boundary condition with the only (β,l) mode turned on.

In what follows, for simplicity but without loss of generality, we shall work solely with the case of $m=0$.

3 Numerical construction of ultra cold holographic lattices

A holographic lattice background can be constructed in at least two ways. One way is to introduce a neutral scalar field with the periodic boundary conditions along the spatial direction. We would like to refer to this kind of holographic lattice as the scalar lattice. The other kind of holographic lattice is induced directly by a periodic chemical potential to the

JHEP07(2013)045

gauge field on the boundary, which is referred to as the ionic lattice. This ionic lattice has been discussed earlier but almost always treated perturbatively in [5–9]. In [2] it was treated exactly without the scalar field. Both of these two kinds of holographic lattice can be numerically constructed by the Einstein-Deturck method, which has been detailed in [1, 10, 11]. In order to see the lattice effect on the Fermi surface, we will follow the same route to construct these two kinds of holographic lattice backgrounds with a rather cold temperature.

3.1 The scalar lattice

To construct an ultra cold scalar lattice, let us consider the following gravitational action including a Maxwell field and a neutral scalar field, i.e.,

$$S=\frac{1}{16\pi G_N}\int d^4x\sqrt{-g}\left[R+\frac{6}{L^2}-\frac{1}{2}F_{ab}F^{ab}-2\nabla_a\Phi\nabla^a\Phi-2M^2\Phi^2\right], \tag{3.1}$$

where L is the AdS radius as before, and M is the mass of the scalar field. In what follows, we shall set $L=1$ and $M^2=-2$. Then the equations of motion can be derived from the above action as

$$R_{ab}+3g_{ab}-2\left(\nabla_a\Phi\nabla_b\Phi-\Phi^2g_{ab}\right)-\left(F_{ac}F_b{}^c-\frac{g_{ab}}{4}F_{cd}F^{cd}\right)=0, \tag{3.2}$$

$$\nabla_aF^a_b=0, \tag{3.3}$$

$$\Box\Phi+2\Phi=0. \tag{3.4}$$

Now with the ansatz in eq. (2.19) for our holographic lattice, the asymptotic behavior of the scalar field is

$$\Phi=z\phi=z[\phi_1+z\phi_2+\mathcal{O}(z^2)] \tag{3.5}$$

near the AdS boundary. Furthermore, the periodic structure can actually be induced by setting the source

$$\phi_1(x)=A_0cos(k_0x), \tag{3.6}$$

and keeping the chemical potential fixed as

$$\mu(x)=\mu. \tag{3.7}$$

For our purpose we would like to construct an ultra cold lattice whose temperature is controlled by the parameter μ_1 in eq. (2.23). This can be achieved by solving the coupled Einstein-Maxwell-scalar equations numerically using the Einstein-DeTurck method. Our numerical method is changing the partial differential equations into non-linear algebraic equations by the standard pseudospectral collocation approximation, and then solving them by employing a Newton-Raphson method. As an example, we show a solution to these equations in figure 1 with $A_0=1.5, k_0=2, \mu=\mu_1=2.35$, which corresponds to a lattice with $T/\mu=0.0081$. Note that different from the scalar field whose period is given by $2\pi/k_0$, the corresponding solutions of all the components of the metric as well as the gauge field have a period of π/k_0 along the x direction, which comes essentially from the fact that in our first equation of motion the stress tensor is quadratic in the scalar field Φ. Since the

JHEP07(2013)045

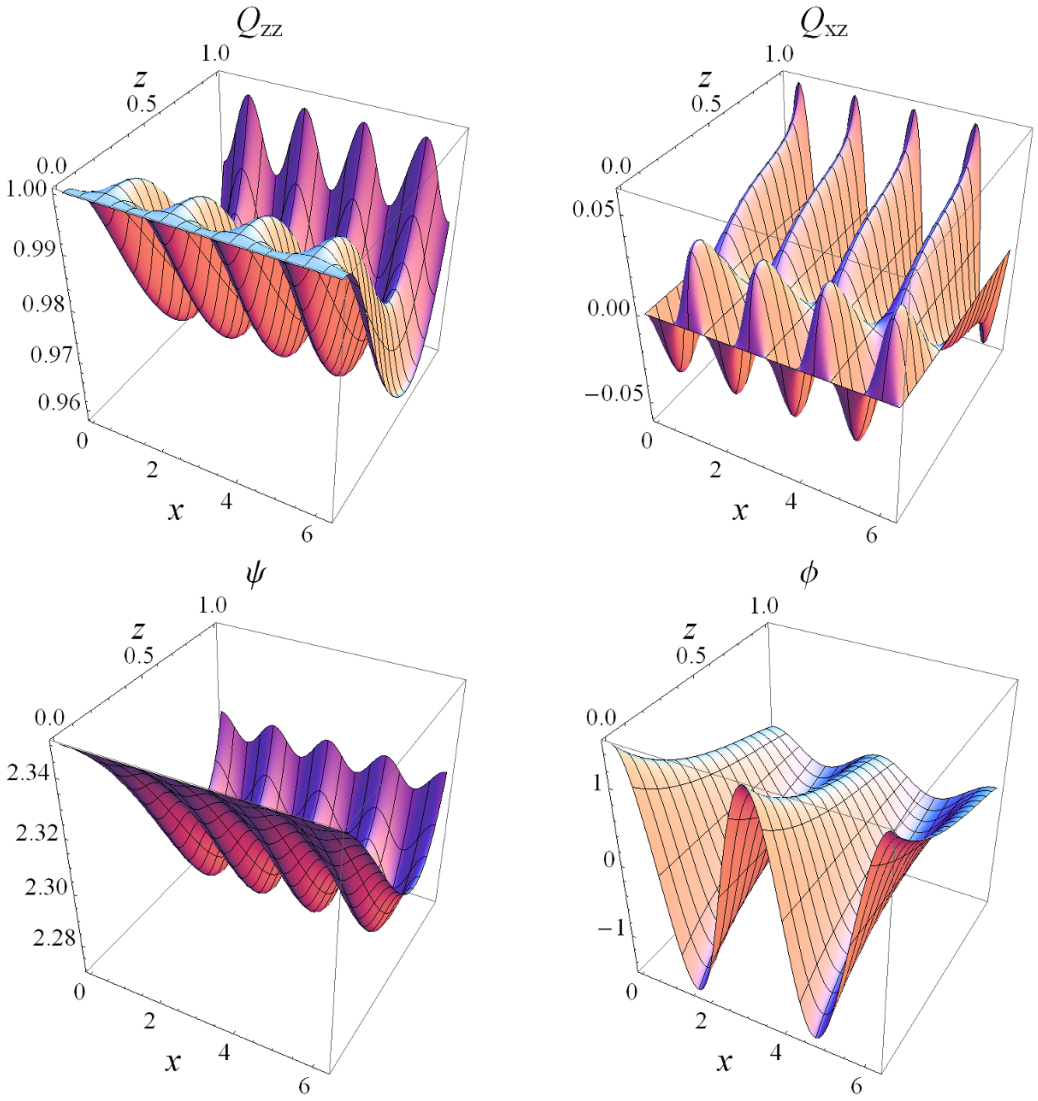

Figure 1. We show Q_{zz}, Q_{xz}, ψ and ϕ for $k_0 = 2$, $A_0 = 1.5$, $\mu = 2.35$ and $T/\mu = 0.0081$.

scalar field does not appear in the Dirac equation, we claim that the lattice constant that the probe Dirac field feel is π/k_0. Therefore, the parameter K in eq. (2.18) is given by $K = 2k_0$.

It is worthwhile to point out that during the course of numerical analysis the lower the temperature is, the harder monitoring the accuracy is. In order to guarantee the convergence of our method at the given temperature, we are required to demonstrate the decaying tendency of the charge discrepancy Δ_N which is defined as $\Delta_N = |1 - Q_N/Q_{N+1}|$ with Q_N the charge on the boundary when the number of grid points takes N. As shown in in figure 2, such a decay is exponential, implying our results are exponential convergence with the increasing of the grid points. Moreover, we have also checked the behavior of the DeTurck vector field ξ^a which is defined in [1] and found that for our solution $\xi^a \xi_a$ is smaller than 10^{-10}, ensuring that our numerics is leading to an Einstein solution rather than a Ricci soliton.

JHEP07(2013)045

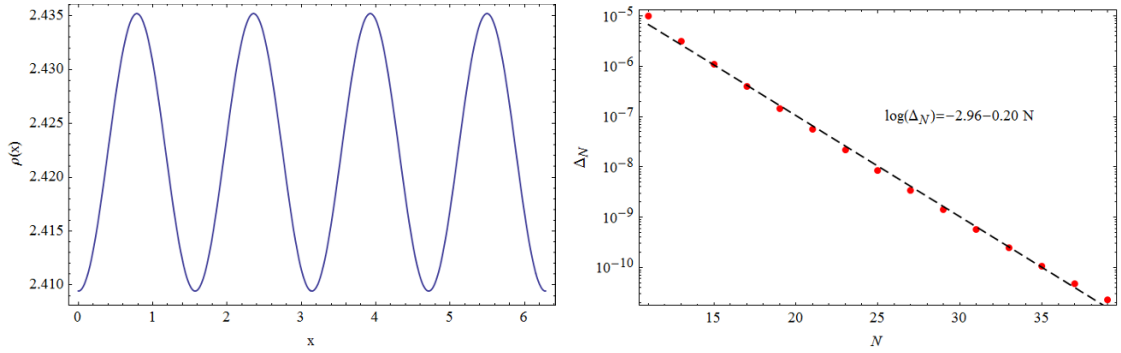

Figure 2. On the left we show the boundary charge density ρ as a function of x, which can be read off by expanding $\psi = \mu + (\mu - \rho)z + \mathcal{O}(z^2)$. On the right we show the charge discrepancy Δ_N as a function of the number of grid points N, where the boundary charge is defined as $Q = \int_0^{2\pi/k_0} dx\rho$. The vertical scale is logarithmic, and the data is well fit by an exponential decay: $\log(\Delta_N) = -2.96 - 0.20\,N$.

3.2 The ionic lattice

Compared to the scalar lattice, the ionic lattice can be generated simply by turning off the scalar field in (3.1) and imposing the spatially varying boundary condition for the chemical potential as

$$\psi(x, 0) = \mu[1 + A_0 cos(k_0 x)]. \tag{3.8}$$

As an example, we illustrate a solution of Q_{xz} and ψ in figure 3 with $k_0 = 2$, $A_0 = 0.1$, $\mu = \mu_1 = 2.3$, which corresponds to $T/\mu = 0.01$. We stress that this type of solutions are different from those for the scalar lattice. Namely the chemical potential is periodic rather than a constant in the scalar lattice. As a result, the boundary charge density in the ionic lattice is expected to vary more dramatically than that in the scalar lattice. This can easily be seen in our plot for the charge density in figure 3. In this sense, one will also expect that the effect onto the Fermi surface due to the ionic lattice should be much stronger than that due to the scalar lattice. We shall show in the subsequent section that this is actually the case.

4 Numerical results for the Fermi surface

The existence of Fermi surfaces for holographic fermionic liquids has been shown in various circumstances. We refer to [12] and [13] for a recent review. In this paper we focus on reporting the following two new results relevant to the Fermi surface when a lattice is introduced for the gravitational background. One is the shape of Fermi surface. In general one expects that the shape of Fermi surface is not circular any more since the rotation symmetry is broken in the presence of the lattice along the x direction. But how the Fermi surface would change appears obscure since the Dirac equation becomes very complicated in this case. Even in the case in which the lattice effect can be treated by conventional condensed matter approach, there is no some kind of universal result on the shape of Fermi surface. Instead the shape will depend on the specific behavior of periodic potential. Nevertheless to our surprise, our numerical analysis gives us a very simple and elegant

JHEP07(2013)045

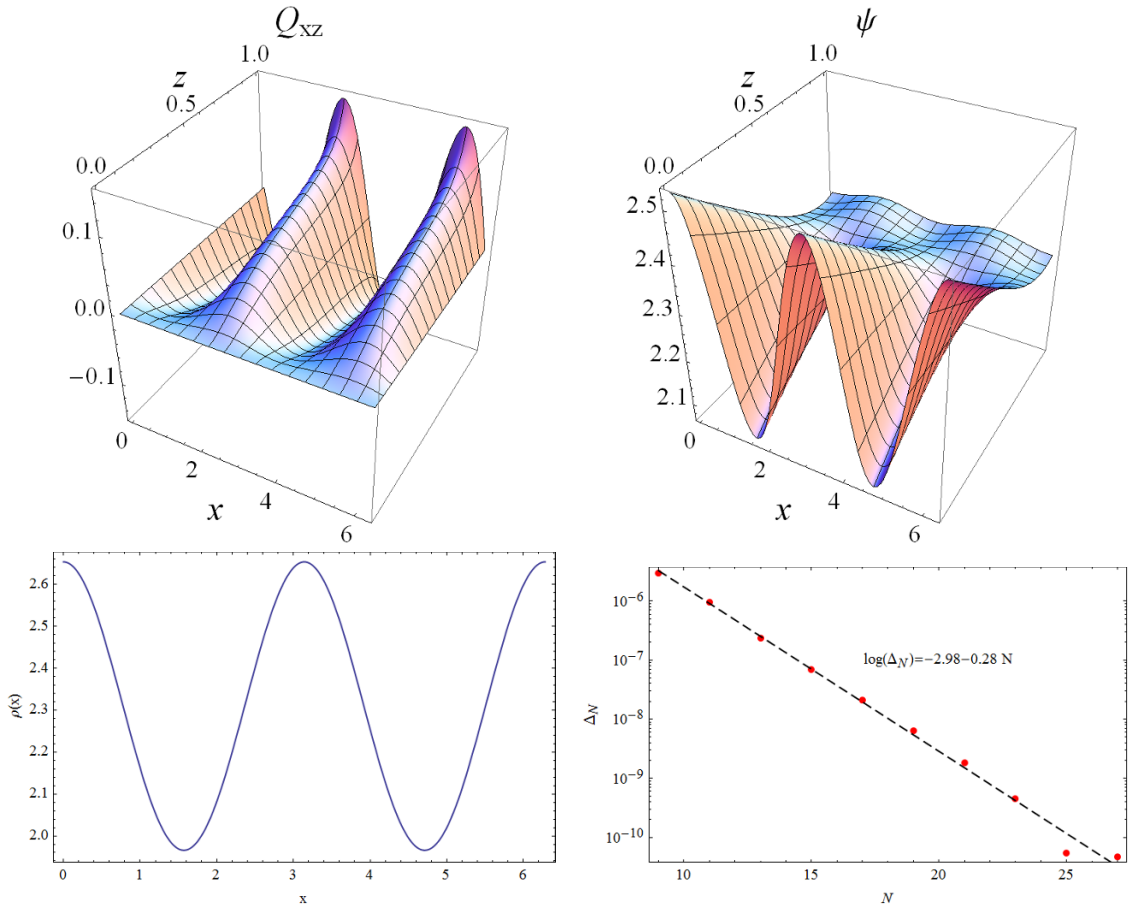

Figure 3. We show Q_{xz} and ψ for $k_0 = 2$, $A_0 = 0.1$, $\mu = 2.3$ and $T/\mu = 0.01$ in the top and the corresponding boundary charge density as well as the tendency of charge discrepancy in the bottom.

answer to this issue. That is, when our holographic Fermi surface is located within the first Brillouin zone, the shape is always an ellipse irrespective of the specific value of parameters in question. The other is the emergence of band gap at the intersection of the Fermi surface with the Brillouin zone boundary. This phenomenon coincides perfectly with the familiar lattice effect as one expects. Now let us demonstrate our numerical results in detail.

To proceed, we would like to remark on how to identify the Fermi surface in our current setting. Note that we are working with holographic fermionic liquid in the presence of lattice at very low but non-zero temperature, where the Fermi surface is somewhat ill defined, because the concept of Fermi surface can only be defined at zero temperature with translation symmetry unbroken. However, as pointed out in [7], the ARPES experiment is actually blind to the lattice by smearing it into a continuum. The measured spectral function can be captured by the imaginary part of diagonal components of retarded Green function, namely $A(\omega, k_x = k_1 + nK, k_y = k_2) = \mathbf{Im}(G_{1,n;1,n} + G_{2,n;2n})$. Furthermore, taking into account that our ultra cold lattice only smears the Fermi surface in a negligible way, we can locate the position of Fermi surface by searching the peak of $A(\omega, k_x, k_y)$ with the tiny frequency ω in the momentum space. Such an identification of Fermi surface is also described in [14] and similar to the operational definition given in [15].

JHEP07(2013)045

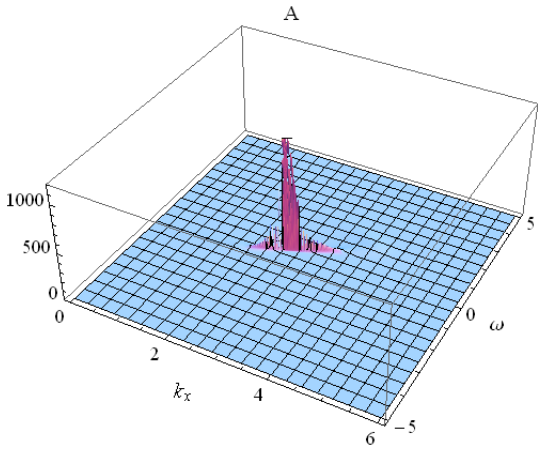

Figure 4. We show the 3d plot of $A(\omega, k_x, 0)$ for $k_0 = 2$, $A_0 = 1.5$, $\mu = 2.35$, $T/\mu = 0.0081$ and $q = 1.7$. A sharp peak near $\omega = 0$ implies a Fermi surface with the Fermi momentum $k_F = 2.634$.

With this in mind, we show in figure 4 an example with the 3d plot of $A(\omega, k)$ for the fixed $k_y = 0$. A sharp peak occurs near $\omega = 0$, indicating a Fermi surface with the Fermi momentum $k_F = 2.634$. Similarly, we may locate the positions of the Fermi surface for other values of k_y such that the shape of the Fermi surface can be plotted in the momentum space. We illustrate our results in figure 5 for the case of $k_0 = 2$, $A_0 = 2$, $\mu = 2.35$, $T/\mu = 0.0081$ and $q = 1.3$, which corresponds to a Fermi surface located within the first Brillouin zone, namely $k_F < K/2 = 2$. Although the shape of Fermi surface appears like a circle in the plot, our data clearly tells us that it is not a circle any more. As a matter of fact, it can be precisely fit by an equation of ellipse as follows

$$\frac{k_x^2}{a^2} + \frac{k_y^2}{b^2} = 1 \tag{4.1}$$

with $a = 1.8991$ and $b = 1.8511$. We find this fitting has a very high accuracy, which can be seen from our error bar analysis presented on the right side of figure 5. Remarkably such a result is universal in the sense that our elliptical Fermi surface is robust against the values of parameters in question except that the longer axis as well as the shorter axis is varied as it should be. Now let us see how our elliptical Fermi surface varies with our relevant parameters. As such, we introduce two quantities, namely, the difference between the longer axis and shorter axis $d = a - b$ as well as the eccentricity $e = \sqrt{a^2 - b^2}/a$. The relevant results are listed in table 1, 2, and 3. Obviously, we observe the following behaviors

- As we increase the amplitude of our periodic source A_0, both d and e are increased.
- As we lower the temperature by increasing μ_1, both d and e are increased.
- As we increase the charge q, the Fermi surface is enlarged with e suppressed.

JHEP07(2013)045

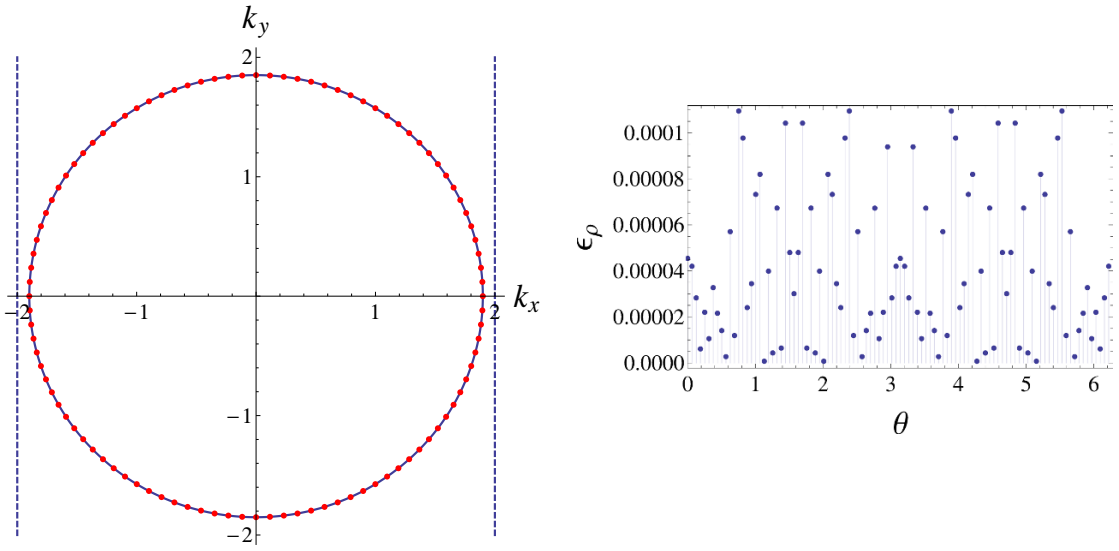

Figure 5. We show the shape of Fermi surface on the left and the error bar fit by the ellipse in the polar coordinate on the right for $k_0 = 2$, $A_0 = 2$, $\mu = 2.35$, $T/\mu = 0.0081$ and $q = 1.3$, where the Fermi momenta $k_F < 2$, namely the Fermi surface is located within the first Brillouin zone.

A_0	0.5	1	1.5	2	2.5
d	0.004	0.013	0.029	0.048	0.069
e	0.06414	0.1187	0.1742	0.2242	0.2675

Table 1. The variation of d and e with the amplitude A_0, where we have fixed the other parameters as $k_0 = 2$, $\mu = 2.35$, $T/\mu = 0.0081$ and $q = 1.3$.

μ_1	2	2.1	2.2	2.3	2.4
d	0.019	0.021	0.024	0.027	0.031
e	0.1487	0.1546	0.1610	0.1696	0.1792

Table 2. The variation of d and e with the temperature which is controlled by μ_1, where we have fixed the other parameters as $k_0 = 2$, $A_0 = 1.5$, $\mu = 2.35$ and $q = 1.3$.

q	0.5	0.7	0.9	1.1	1.3
d	0.013	0.018	0.022	0.026	0.029
e	0.2479	0.2258	0.2010	0.1871	0.1742

Table 3. The variation of d and e with the charge q, where we have fixed the other parameters as $k_0 = 2$, $A_0 = 1.5$ and $\mu = \mu_1 = 2.35$.

We remark that above phenomena can be observed in the ionic lattice background as well. Interestingly, we find that in ionic lattice case, the longer axis of the ellipse changes from x to y direction.

When the charge q is large enough, the Fermi surface will go beyond the first Brillouin zone with $k_F > K/2$. Now let us turn to such a situation by first demonstrating the band

JHEP07(2013)045

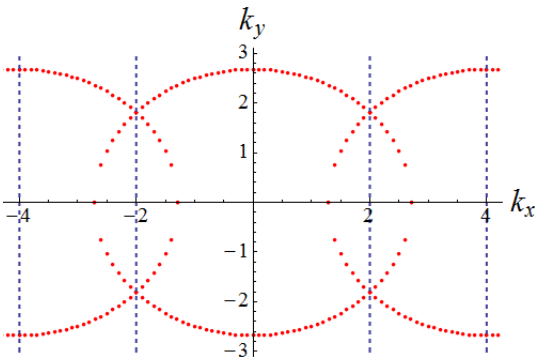

Figure 6. Band structure for $q = 1.7$,$k_0 = 2$, $A_0 = 1.5$ and $\mu = \mu_1 = 2.35(k_F > 2)$.

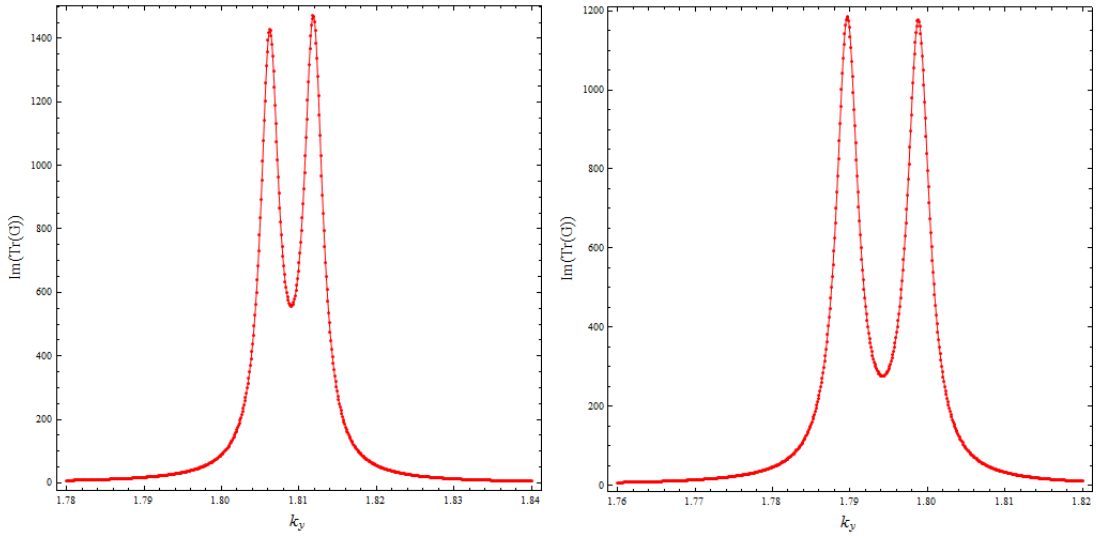

Figure 7. There are two peaks for the imaginary part of the Green function at $k_x = 2$(BZ boundary). The left one is for $A_0 = 1.5$ while the right one for $A_0 = 2$, with $q = 1.7$,$k_0 = 2$, and $\mu = \mu_1 = 2.35$ fixed.

structure of Fermi surface in figure 6 for the scalar lattice. Note that the Fermi surface exhibits a periodic structure along the k_x direction as it should be the case guaranteed by Bloch theorem. On the other hand, it appears that our Fermi surface does not show the band gap structure at the intersection of the Fermi surface with the Brillouin zone boundary, which is at odds with the familiar lattice effect. In order to see if this is really the case, we zoom in the Fermi surface precisely at the Brillouin zone boundary. The corresponding result is plotted in figure 7. To our pleasure, the band gap shows up and becomes large with the increase of the amplitude of periodic source. So to see a clearer band gap structure, it

JHEP07(2013)045

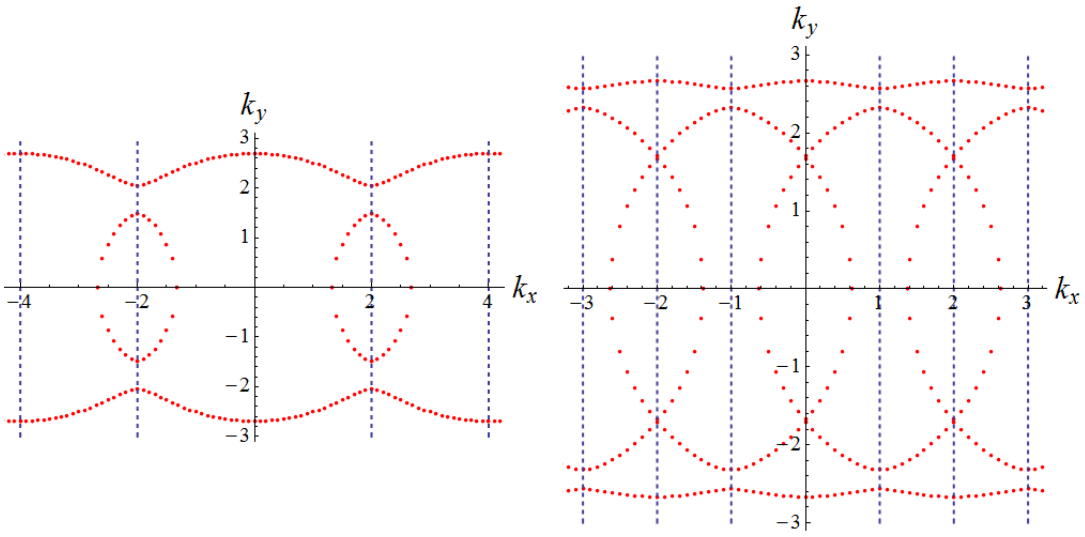

Figure 8. Band structure in ionic lattice model for $k_F > K/2(q = 1.7, A_0 = 0.3, \mu = \mu_1 = 2.3)$ and $k_F > K(q = 1.7, A_0 = 0.1, \mu = \mu_1 = 2.3)$. Note that for the left one we have set $k_0 = 4$ such that $K = 4$, while for the right one $k_0 = 2$ such that $K = 2$.

is better to move on to the ionic lattice in which the lattice effects should be much stronger as we discussed in previous section. As shown in figure 8 for the ionic lattice, the gap is evidently observed as one expects. From this figure we also notice that the band structure becomes richer when the Fermi surface intersects with more than two Brillouin zones.

5 Conclusion

We have investigated the lattice effect on the Fermi surface by putting the bulk Dirac field in the ultra cold holographic lattices, where both the background equations and the probe Dirac field are solved by pseudo-spectral method numerically. One interesting result is that the Fermi surface is always modified by the lattice from a circle to an ellipse. Suppose that such a Fermi surface is formed by some kind of exotic free fermionic quasi-particles, then the elliptical shape means that the effective mass along the x direction in scalar lattice (or the y direction in ionic lattice) becomes more massive by some kind of renormalization effects due to the presence of the lattice. In any case, such a universal behavior of holographic Fermi surface begs for a deeper understanding. In addition, we holographically reproduce the band gap structure at the intersection of the Fermi surface and the Brillouin zone boundary, which is a well known lattice effect on the Fermi surface in condensed matter theory.

Note that such a band gap structure is also obtained in [7]. We would like to compare our work with [7]. The lattice considered in that paper is a weak ionic lattice, where the back reaction of the periodic chemical potential to the bulk geometry is ignored. The advantage of such a weak potential limit is two fold. One is that such a lattice can be put at zero temperature, and the other is that the analytic technique developed in [4] can be borrowed heavily to the relevant perturbation calculation. The disadvantage is also obvious. First, the amplitude of spatially varying chemical potential must be small enough, other-

JHEP07(2013)045

wise the perturbation calculation will break down. Second, the neglect of the back reaction may lead to the loss of some significant physics. For example, the elliptical Fermi surface we find does not appear in the perturbation calculation.[1] Third, when such a perturbation calculation is made to higher order or for the non-diagonal components of retarded Green function, the analysis will become much involved. Compared with this, the full retarded Green function can be obtained by our numerics once and for all. In this sense, our paper and [7] are complementary to each other.

We conclude with various issues worthy of further investigation. First, even though it is numerically harder, it is apparently better to construct the zero temperature holographic lattices for our probe Dirac field to propagate in. Second, pertaining to the STM experiment, it is important for us to extract the retarded Green function in the position space, which can be achieved in the following two ways. One is to Fourier transform our resultant Green function in the momentum space to the position space. The other is to work directly in the position space by imposing Dirac delta source on the AdS boundary. We hope to address these issues in the near future.

Acknowledgments

We are grateful to Liqing Fang, Xianhui Ge, Xiaomei Kuang, Yan Liu, Yu Tian, Bin Wang, Shaofeng Wu and Xiaoning Wu for helpful discussions. This work is supported by the Natural Science Foundation of China under Grant Nos.11275208 and 11178002. Y.L. also acknowledges the support from Jiangxi young scientists (JingGang Star) program and 555 talent project of Jiangxi Province. J.W. is also supported by the National Research Foundation of Korea(NRF) grant funded by the Korea government(MEST) through the Center for Quantum Spacetime(CQUeST) of Sogang University with grant number 2005-0049409. H.Z. is supported in part by the Belgian Federal Science Policy Office through the Interuniversity Attraction Pole P7/37, by FWO-Vlaanderen through the project G.0114.10N, and by the Vrije Universiteit Brussel through the Strategic Research Program "High-Energy Physics".

References

[1] G.T. Horowitz, J.E. Santos and D. Tong, *Optical conductivity with holographic lattices*, *JHEP* **07** (2012) 168 [arXiv:1204.0519] [INSPIRE].

[2] G.T. Horowitz, J.E. Santos and D. Tong, *Further evidence for lattice-induced scaling*, *JHEP* **11** (2012) 102 [arXiv:1209.1098] [INSPIRE].

[3] G.T. Horowitz and J.E. Santos, *General relativity and the cuprates*, arXiv:1302.6586 [INSPIRE].

[4] T. Faulkner, H. Liu, J. McGreevy and D. Vegh, *Emergent quantum criticality, Fermi surfaces and AdS_2*, *Phys. Rev.* **D 83** (2011) 125002 [arXiv:0907.2694] [INSPIRE].

[1] Of course, such a Fermi surface may show up when one goes to higher order in the perturbation calculation. After all, the perturbation calculation is made only to second order in [7].

JHEP07(2013)045

[5] S.A. Hartnoll and D.M. Hofman, *Locally critical resistivities from Umklapp scattering*, *Phys. Rev. Lett.* **108** (2012) 241601 [arXiv:1201.3917] [INSPIRE].

[6] K. Maeda, T. Okamura and J.-I. Koga, *Inhomogeneous charged black hole solutions in asymptotically anti-de Sitter spacetime*, *Phys. Rev.* **D 85** (2012) 066003 [arXiv:1107.3677] [INSPIRE].

[7] Y. Liu, K. Schalm, Y.-W. Sun and J. Zaanen, *Lattice potentials and fermions in holographic non Fermi-liquids: hybridizing local quantum criticality*, *JHEP* **10** (2012) 036 [arXiv:1205.5227] [INSPIRE].

[8] R. Flauger, E. Pajer and S. Papanikolaou, *A striped holographic superconductor*, *Phys. Rev.* **D 83** (2011) 064009 [arXiv:1010.1775] [INSPIRE].

[9] J.A. Hutasoit, G. Siopsis and J. Therrien, *Conductivity of strongly coupled striped superconductor*, arXiv:1208.2964 [INSPIRE].

[10] M. Headrick, S. Kitchen and T. Wiseman, *A new approach to static numerical relativity and its application to Kaluza-Klein black holes*, *Class. Quant. Grav.* **27** (2010) 035002 [arXiv:0905.1822] [INSPIRE].

[11] P. Figueras, J. Lucietti and T. Wiseman, *Ricci solitons, Ricci flow and strongly coupled CFT in the Schwarzschild Unruh or Boulware vacua*, *Class. Quant. Grav.* **28** (2011) 215018 [arXiv:1104.4489] [INSPIRE].

[12] T. Faulkner, N. Iqbal, H. Liu, J. McGreevy and D. Vegh, *Holographic non-Fermi liquid fixed points*, arXiv:1101.0597 [INSPIRE].

[13] N. Iqbal, H. Liu and M. Mezei, *Lectures on holographic non-Fermi liquids and quantum phase transitions*, arXiv:1110.3814 [INSPIRE].

[14] F. Benini, C.P. Herzog and A. Yarom, *Holographic Fermi arcs and a d-wave gap*, *Phys. Lett.* **B 701** (2011) 626 [arXiv:1006.0731] [INSPIRE].

[15] A. Kanigel et al., *Evolution of the pseudogap from Fermi arcs to the nodal liquid*, *Nature Phys.* **2** (2006) 447.

JHEP07(2013)045